A Narrow-Linewidth On-Chip Toroid Raman Laser

Tao Lu, Lan Yang, Tal Carmon, and Bumki Min

***Abstract*— In this paper, we report a narrow-linewidth on-chip toroid Raman laser. Under free-running condition, we have obtained the minimum fundamental linewidth of 3 Hz and the maximum unidirectional output power of 223 μW. Lasing under the same condition in continuous-wave mode over 90 min is achieved at an average power level of 21 μW and a standard deviation of 0.17 μW. We further derived the frequency noise spectrum and identified an enhancement of frequency noise due to Kerr nonlinearity. In addition, we have observed the shifting of relaxation oscillation frequency as a consequence of weak mode splitting.**

***Index Terms*— Laer noise, optical resonators, phase noise, Raman lasers.**

I. Introduction

NARROW-LINEWIDTH on-chip lasers are critical components in lab-on-a-chip devices to reduce the chromatic dispersion in high-resolution measurements. They are also indispensable in coherent optical communication, where highly coherent sources are necessary for phase modulation formats. Currently, ultranarrow-linewidth laser sources [1], [2] are available, but none of them can be integrated on a silica-on-silicon chip through monolithic integration. On the other hand, no ultranarrow-linewidth on-chip lasers [3], [4] have been reported due to the combined difficulties of fabricating an on-chip ultrahigh-quality-factor (Q) resonant cavity and measuring a linewidth at several hertz (Hz) in the presence of frequency drift during a single measurement. In 2003, a toroid-shaped silica microcavity on a silicon wafer with Q as high as 500 million was fabricated [5]. Since then, a narrow-linewidth Erbium-doped toroid laser has been demonstrated [6]. Although it has been shown that the potential laser linewidth can reach several Hz both theoretically and experimentally, the coexistence of splitting modes [7], [8] in one single toroid makes it difficult to implement a more reliable heterodyne measurement procedure using two independently pumped lasers. Recently, we investigated the frequency noise structure of on-chip toroid-based Raman lasers in [9]–[12]. We were able to obtain a single-mode Raman toroid laser by fabricating a "fat" toroid on a thermal silica wafer. The optical power density at the splitting frequency was below −155 dBc/Hz, in contrast to the Erbium lasers where an equal power of the split lasing modes can be reached. In this paper, we report the fundamental linewidth of a Raman laser as low as 3 Hz with a maximum unidirectional output power of 223 μW. The fundamental linewidth is the lowest among all on-chip laser sources to date, to the best of our knowledge. We further investigated the "technical noise" of the laser, and observed a frequency noise enhancement from the pump intensity fluctuation due to Kerr nonlinearity and self-phase modulation, both experimentally and analytically.

Manuscript received June 9, 2010; revised September 27, 2010; accepted October 1, 2010. Date of current version February 24, 2011.

T. Lu is with the Department of Electrical and Computer Engineering, University of Victoria, Victoria, BC V8P 5C2, Canada (e-mail: taolu@ece.uvic.ca).

L. Yang is with the Department of Electrical and Systems Engineering, Washington University, St. Louis, MO 63130 USA (e-mail: yang@seas.wustl.edu).

T. Carmon is with the University of Michigan, Ann Arbor, MI 48109-2099 USA (e-mail: tcarmon@umich.edu).

B. Min is with the Department of Mechanical Engineering, Korea Advanced Institute of Science and Technology, Daejeon 305-751, Korea (e-mail: bmin@kaist.ac.kr).

Color versions of one or more of the figures in this paper are available online at http://ieeexplore.ieee.org.

Digital Object Identifier 10.1109/JQE.2010.2087742

II. Frequency Noise Spectrum of a Microtoroid Raman Laser

The semiclassical Langevin equation of a microtoroid Raman laser can be modeled as [9], [10], [13], [14]

$$\begin{aligned} \frac{dA_s}{dt} &= -\frac{\gamma}{2}A_s + \frac{g^c}{2}I_p A_s - j\Delta\omega(I_p)A_s + \Delta_s \\ \frac{dI_p}{dt} &= -\gamma_p I_p - \frac{\omega_p}{\omega_s}g^c I_s I_p + B. \end{aligned} \tag{1}$$

The intracavity electric fields of Raman (E_s) and pump (E_p) are expressed as $E_{\{s,p\}}(\vec{r},t) = A_{\{s,p\}}e^{-j\omega_{\{s,p\}}}\hat{E}_{\{n,m\}}(\vec{r},\omega_{\{n,m\}})$. Here, $\hat{E}_{\{n,m\}}(\vec{r},\omega_{\{n,m\}})$ is the corresponding normalized electric field of Raman and pump whispering gallery modes at their corresponding resonance frequencies $\omega_{\{n,m\}}$, at a spatial location $\vec{r}$. $A_{\{s,p\}}(t) = A_{\{s,p\},0}[1+\rho_{\{s,p\}}(t)]e^{j\phi_{\{s,p\}}(t)}$ denote the slow varying electric field envelopes of the Raman (subscript s) and pump (subscript p) modes, and $\rho_{\{s,p\}}$ and $\phi_{\{s,p\}}$ are the amplitude and phase fluctuations. The whispering gallery modes are normalized such that $A_{\{s,p\}}A^*_{\{s,p\}} = I_{\{s,p\}}$ is normalized to the intensity $I_{\{s,p\}}$. Moreover, $\Delta\omega(I_p) = \omega_s - \omega_n$ is the frequency detuning of the Stokes wave as a function of I_p due to cross-phase modulation of the pump laser to the Raman laser, g^c is the cavity-enhanced Raman gain coefficient [9], [10], and $I_{\{s,p\}} \approx I_{\{s,p\},0}(1+2\rho_{\{s,p\}})$ is the corresponding intensity whose relative intensity noise (RIN) is twice its amplitude fluctuation $\rho_{\{s,p\}}$. Similarly, $B(t) = 2\kappa Real\{E_p(t)^* s(t)\}$ is the coupled external pump source $s(t)$ into cavity with coupling coefficient κ. Note that the coupled intensity fluctuation ρ_B is due to both the intensity and phase noises of the external source, $B \approx B_0[1+2\rho_B(I_{in},\Delta\omega_{in})]$, and $\Delta_s = \Delta_{r,s} + i\Delta_{i,s}$ is the Langevin force term of the laser. From (1), and applying standard linearization procedure [15], we obtain

$$\frac{d\rho_s}{dt} = \frac{\omega_s}{Q_s}\rho_p + \frac{\Delta_{r,s}}{A_{s,0}} \tag{2a}$$

$$\frac{d\phi_s}{dt} = -\alpha\frac{\omega_s}{Q_s}\rho_p + \frac{\Delta_{i,s}}{E_s} \tag{2b}$$

$$\frac{d\rho_p}{dt} = -\left(\gamma_p + \frac{\omega_p}{Q_s}\frac{I_{s,0}}{I_{p,0}}\right)\rho_p - \frac{\omega_p}{Q_s}\frac{I_{s,0}}{I_{p,0}}\rho_s + \frac{B_0}{I_{p,0}}\rho_B \tag{2c}$$

where ω_s and Q_s are the angular frequency and the quality factor of Stokes wave, respectively, and $\alpha = 2(\partial\Delta\omega/\partial I_p)/g^c$ characterizes the phase fluctuation coupled from intracavity pump intensity fluctuation due to the Kerr nonlinearity. By taking the Fourier transform of ρ_s, ρ_p and $d\phi_s/dt$, we have

$$\tilde{\rho}_p(\Omega) = \frac{j\Omega\left(\frac{B_0}{2I_{p,0}}\tilde{\rho}_B + \frac{\tilde{\Delta}_p}{2I_{p,0}}\right) - \frac{\omega_p}{Q_s}\frac{I_{s,0}}{I_{p,0}}\frac{\tilde{\Delta}_{r,s}}{E_{s,0}}}{\Omega_R^2 - \Omega^2 + j\Omega/\tau_R} \tag{3a}$$

$$\tilde{\rho}_s(\Omega) = \frac{\omega_s}{Q_s}\frac{\tilde{\rho}_p}{j\Omega} + \frac{\tilde{\Delta}_{r,s}}{j\Omega E_{s,0}} \tag{3b}$$

where the relaxation oscillation frequency $\Omega_R = \left(I_{s,0}\omega_p\omega_s/I_{p,0}Q_s^2\right)^{1/2}$, and $\tau_R = 1/[\gamma_p + (\omega_p/Q_s)(I_{s,0}/I_{p,0})]$. Consequently, the intracavity laser W_s and pump W_p RINs are expressed as

$$W_p(\Omega) = 4\tilde{\rho}_p\tilde{\rho}_p^* = \frac{\Omega^2\left(\frac{B_0}{2I_{p,0}}\tilde{\rho}_B + \frac{\tilde{\Delta}_p}{2I_{p,0}}\right)^2 + \left(\frac{\omega_p}{Q_s}\frac{I_{s,0}}{I_{p,0}}\right)^2\omega_{ST}}{\left(\Omega_R^2 - \Omega^2\right)^2 + \frac{\Omega^2}{\tau_R^2}} \tag{4a}$$

$$W_s(\Omega) = \left(\frac{\omega_s}{Q_s}\right)^2\frac{W_{\rho_p}}{\Omega^2} + \frac{\omega_{ST}}{\Omega^2}. \tag{4b}$$

The frequency noise spectrum $S_{\Delta\nu}$ has the form

$$S_{\Delta\nu}(\Omega) = \alpha^2\frac{\omega_s^2}{Q_s^2}W_{\rho_p} + 2\pi\Delta\nu_{ST} \tag{5}$$

where $\Delta\nu_{ST}$ is the quantum-noise-limited Schawlow–Townes [16] linewidth, defined as the quantum fluctuation of the laser phase due to spontaneous emissions. The fundamental linewidth $\Delta\nu_{ST}$ in a laser can be obtained as [17]–[19]

$$\Delta\nu_{ST} = \frac{2\pi\mu h\nu^3}{PQ_TQ_L} = \frac{2\pi(1+K_Q)K_Q h\nu^3}{PQ_0^2}. \tag{6}$$

It is inversely proportional to the laser power P and to the square of laser cold cavity quality factor Q_0. Here, Q_T is the total quality factor, Q_C is the coupling related Q, and Q_0 is the intrinsic quality factor, $K_Q = Q_0/Q_L$. As the fundamental linewidth of a laser is inversely proportional to the square of the quality factor Q of the resonant cavity, an ultrahigh-Q-cavity-based laser will reduce the fundamental linewidth significantly. In our laser system, the cold cavity Q of the Raman toroid pump mode under test is well above 10^8, and the Raman lasing mode Q is on the order of 10^7. A total output lasing power as high as 223 μW in one direction is recorded.

A. Influence of Backscattering and Kerr Nonlinear Effects

When light propagates inside an ultrahigh-Q cavity in one direction, minute backscattering can easily overcome the round-trip loss to establish a resonant field in the backward direction [7]

$$\begin{aligned}\frac{dA_{s+}}{dt} &= \tfrac{g^c}{2}(I_{p+}+I_{p-})A_{s+}(t) - \tfrac{\gamma}{2}A_{s+}(t) + j\beta_s A_{s-}(t)\\ &\quad + j\Delta\omega(I_{s+}, I_{s-}, I_{p+}, I_{p-})A_{s+} + \Delta_{s+}\\ \frac{dA_{s-}}{dt} &= \tfrac{g^c}{2}(I_{p+}+I_{p-})A_{s+}(t) - \tfrac{\gamma}{2}A_{s-}(t) + j\beta_s A_{s+}(t)\\ &\quad + j\Delta\omega(I_{s+}, I_{s-}, I_{p+}, I_{p-})A_{s-} + \Delta_{s-}\end{aligned} \tag{7}$$

where A_{s+} and A_{s-} are the amplitudes of the forward (+) and backward (−) propagating mode of the Stokes components, I_{p+} and I_{p-} are the pump intensity in the forward and backward directions, $\Delta\omega$ is the frequency detuning due to the cross-phase modulation of the pump field and the self-phase modulation from the Stokes field, and $\beta_s = |\beta_s|e^{-j\Delta} = \omega_s/2(< E_n|\delta\epsilon_r|E_n > / < E_n|\epsilon_r|E_n >)$. Equation (7) can be decoupled according to the linear transformation

$$\begin{pmatrix} A_{cos} \\ A_{sin} \end{pmatrix} = \frac{1}{\sqrt{2}}\begin{pmatrix} e^{j\frac{\Delta}{2}} & e^{-j\frac{\Delta}{2}} \\ e^{j\frac{\Delta}{2}} & -e^{-j\frac{\Delta}{2}} \end{pmatrix}\begin{pmatrix} A_{s+} \\ A_{s-} \end{pmatrix} \tag{8}$$

to form two spatially orthogonal modes A_{cos} and A_{sin}, where the subscript cos and sin represent cosine and sine Stokes modes. These two modes have a frequency split of $|\beta_s|$ and therefore referred to as split frequency. Similarly, the forward and backward pumps form cosine and sine modes. As the laser is pumped by a single-frequency tunable laser source, here, for simplicity, we assume the cosine mode of the pump is excited inside the cavity and $I_{p,cos} \equiv I_p$. Hence

$$\frac{dI_p(t)}{dt} = -\frac{\omega_p}{\omega_s}g^c\left[I_{cos}(t) + I_{sin}(t)\right]I_p(t) - \gamma_p I_p + B. \tag{9}$$

Linearizing the above dynamic equations through similar procedures mentioned previously, we obtain

$$\begin{aligned} W_p(\Omega) &= \frac{\frac{\omega_p^2}{Q_c^2}2\pi\nu_{ST}\left(h_c^2 + h_s^2\right) + \Omega^2\frac{|B_0|^2}{|I_{p0}|^2}W_B(\Omega)}{\left(\Omega_R^2 - \Omega^2\right)^2 + \frac{\Omega^2}{\tau_R^2}}\\ W_{cos}(\Omega) &= W_{sin}(\Omega) = \frac{1}{4\Omega^2}\frac{\omega_s^2}{Q_s^2}W_p(\Omega) + \frac{1}{\Omega^2}2\pi\Delta\nu_{ST}. \end{aligned} \tag{10}$$

Therefore, the RIN spectrum of the forward propagating wave $W(\Omega) \equiv W_+(\Omega)$ is given by

$$\begin{aligned} W(\Omega) &= \pi^2\delta^2(0) + \frac{I_{c0}^2 + I_{s0}^2}{4\left(I_{c0}+I_{s0}\right)^2}W_{cos}(\Omega)\\ &\quad + \frac{4\pi^2 I_{c0}I_{s0}}{\left(I_{c0}+I_{s0}\right)^2}\left[\delta^2(\Omega - |\beta_s|) + \delta^2(\Omega + |\beta_s|)\right]\\ &\quad + \frac{2\pi^2 I_{c0}I_{s0}}{\left(I_{c0}+I_{s0}\right)^2}\left[W_{cos}(\Omega + |\beta_s|) + W_{cos}(\Omega - |\beta_s|)\right]. \end{aligned} \tag{11}$$

Compared to the relaxation oscillation, the new relaxation oscillation frequency Ω_R^+ is upconverted by the split frequency $|\beta_s|$, creating side bands both above and below $|\beta_s|$ by an amount of Ω_R defined in the previous section.

Finally, we obtain the modified frequency noise spectrum of the Raman laser as

$$S_{\Delta\nu}(\Omega) = \frac{\alpha^2}{4}\frac{\omega_s^2}{Q_s^2}W_p(\Omega) + \frac{9\alpha^2}{16}\frac{\omega_s^2}{Q_s^2}\frac{I_{s,0}^2}{I_{p,0}^2}W(\Omega) + 2\pi\,\Delta\nu_{ST}. \tag{12}$$

B. Quantum Mechanical Modification

As the semiclassical model derived above fails to predict the quantum noise floor of both the intracavity pump and laser intracavity intensity noise, a more accurate treatment should be considered using a quantum mechanical model [20]. Physically, the existence of such quantum noise will be coupled to the fundamental frequency noises through Kerr nonlinearity. As such coupling is instantaneous, the fundamental linewidth should be modified according to

$$\Delta\nu_{ST} = \frac{2\pi\mu h\nu^3}{PQ_TQ_L} = (1+\alpha^2)\frac{2\pi(1+K_Q)K_Q h\nu^3}{PQ_0^2}. \tag{13}$$

C. Pump Frequency Jitter-Induced Fluctuation

In the case of a passive cavity, when a pump laser at optical frequency f_0 establishes a resonance intracavity intensity I_0, the following cavity resonance condition has to be satisfied, $(n_0 + n_2)I_0L_{eff} = m(c/f_0)$, where n_0 is the refractive index of the cavity material, n_2 is the Kerr coefficient and, c is the speed of light. In the presence of frequency jitter δf, we have the intracavity pump intensity fluctuation $\delta I = (n_0 + n_2I_0/n_2)(\delta f/f_0)$. Assuming that the external pump power P_{in} is critically coupled to the cavity, the RIN is given by

$$RIN = \frac{\pi n_0^2 L A_{eff}}{n_2\lambda Q_0 P_{in}}\frac{\delta f}{f_0}. \tag{14}$$

A typical value of $Q_0 = 2\times10^7$ and $P_{in} = 1$ mW yields 2% RIN. At frequencies below 100 kHz, thermal effects may further enhance the fluctuation, whereas at frequencies above 100 kHz, this Kerr-induced fluctuation will be dominant and the corresponding noise bandwidth is only limited by the frequency jitter bandwidth.

In cavity Raman lasers, the frequency jitter causes fluctuation in the intracavity pump power, which will be transferred to the frequency jitter of the Stokes components through cross-phase modulation. The Raman frequency jitter will further introduce additional intensity fluctuation due to the same (14) and enhance the frequency noise through self-phase modulation. A detailed modeling of this mechanism is out of the scope of this paper and will be discussed in a forthcoming paper.

III. Ultranarrow-Linewidth Measurement Using the Coherent Discriminator Method

Conventionally, when the linewidth is large compared to the frequency drift, the linewidth can be measured by heterodyning to a reference laser of at least similar linewidth, yielding a Lorentzian-shaped power spectrum of the beat note. The spectrum can then be acquired by an RF spectrum analyzer [21]. The full-width at half-maximum of the Lorentzian peak is the total linewidth of both lasers. To accurately measure the linewidth, the resolution bandwidth or the inverse of the acquisition time of the spectrum analyzer has to be set at least smaller than the linewidth. Therefore, to measure a laser linewidth below kilohertz, the acquisition time of the spectrum analysis needs to be set to longer than milliseconds. The frequency drift in the acquisition window is usually small and will not broaden the spectrum noticeably. As the linewidth decreases, the acquisition time of the spectrum analyzer will increase accordingly, resulting in an increase in the amount of frequency drift in the acquisition window. When the frequency drift is larger than the linewidth, the spectrum of the beat note will be dominated by the Gaussian-shaped frequency drift spectrum and the linewidth cannot be resolved. Therefore, the conventional heterodyne technique is not applicable for ultranarrow-linewidth measurements.

In our experiment, we apply coherent discriminator methods [21], which employ an optical frequency discriminator, to overcome the frequency drift due to the long acquisition time in conventional methods. We set up a homodyne technique using optical delay lines as the frequency discriminator.

A. Optical Discriminator Method

The experimental setup of the optical discriminator method is shown in Fig. 1(a). A toroid is pumped at a wavelength around 1450 nm using a new focus-tunable laser to generate a Raman lasing mode at around 1550 nm. Ten percent of the lasing power is monitored through a 10/90 optical coupler, while the remaining 90% is then split equally through a 50/50 coupler and passes through an optical frequency discriminator formed by an optical delay line and an optional acousto-optical modulator (Brimose) to differentiate the phase noise from the intensity noise at the cost of additional signal attenuation. (We did not use it here due to relatively low power of our signal. Adoption of such device is highly recommended for ultranarrow-linewidth measurement for higher resolution.) The two branches are then recombined through another 50/50 coupler. The output signal is detected through a balanced detector (Thorlabs PDB120C), and its power density spectrum is captured by a Tectronix 3408A real-time spectrum analyzer. Meanwhile, a real-time oscilloscope (Agilent 54854A) is used to trigger the analyzer at the quadrature point.

The operating principle of the optical discriminator is as follows. Assume that the electric field of the Raman laser has the form $E_{in}(t) = E_0[1+\rho(t)]e^{j[\omega t+\phi(t)]}$ in front of the optical frequency discriminator and the two optical couplers have power splitting ratios α_1 and α_2 which are close to 0.5. At the output of the discriminator, after passing through the optical delay line with differential delay τ_D, it can be shown that the photocurrents I_1 and I_2 normalized to their peak to peak value I_{pp} are given by

$$\begin{aligned}\frac{I_1}{I_{pp}} &= \alpha_1\alpha_2\,[1+\rho(t-\tau_D)]^2 + (1-\alpha_1)(1-\alpha_2)\\ &\quad [1+\rho(t)]^2 - 2\sqrt{\alpha_1\alpha_2(1-\alpha_1)(1-\alpha_2)}\\ &\quad \cos[\omega\tau_D + \Delta\phi(t,\tau_D)]\end{aligned}$$

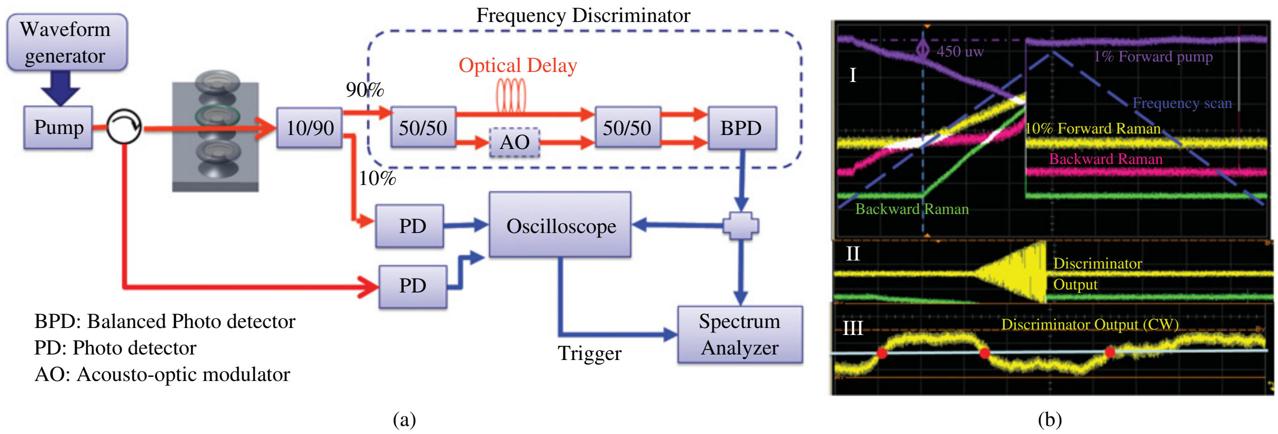

Fig. 1. (a) Schematic of the experimental setup. The pump laser is coupled to a silica toroid through a tapered fiber. The Raman laser is coupled out from the toroid to the same taper in both forward and backward directions. The forward-propagating Raman laser is split into two branches with a 90/10 directional coupler, the power at the 10% arm is monitored as a reference to the signal power, and the 90% arm is coupled to the optical frequency discriminator to convert the frequency fluctuation of the laser into amplitude variation. The optical signal is then converted to an electrical signal via a balanced detector and the corresponding laser frequency noise spectrum is derived from the power spectral density (PSD) recorded by an electrical spectrum analyzer. The backward-propagating Raman laser is also monitored by an optical circulator. The optical frequency discriminator illustrated in the dashed block is formed by a 50/50 coupler, with one of its arm connected to an optical delay line, the signals are then recombined through another 50/50 coupler. Optionally, an accustooptic modulator can be inserted into one of the arm to further suppress the residual intensity noise from the frequency noise spectrum. (b) Inset I: Oscilloscope traces of 1% pump (purple line) and 10% Raman (yellow line) output powers in the forward direction, pink and green lines show the pump and Raman output powers in the backward directions, the blue dash line represents the scan of tunable laser wavelength. The oscilloscope trace of the discriminator output is displayed in inset II when the pump frequency is in the scan mode and in inset III when it is in the continuous-wave (CW) mode.

$$\frac{I_2}{I_{pp}} = \alpha_1(1-\alpha_2)\,[1+\rho(t-\tau_D)]^2 + (1-\alpha_1)\alpha_2\,[1+\rho(t)]^2 + 2\sqrt{\alpha_1\alpha_2(1-\alpha_1)(1-\alpha_2)}\cos[\omega\tau_D + \Delta\phi(t,\tau_D)]. \quad (15)$$

The last term on the right hand side of (15) contains the phase noise information, while the first two terms are dominated by intensity noises. In our experiment, we use a balanced detector that subtracts the photocurrent of the two arms to significantly reduce the intensity noise. Therefore, after the balanced detector, the output voltage V_{out} normalized to peak-to-peak voltage V_{pp} has the form (assuming that at quadrature point $\omega\tau_D = (2k+1/2)\pi$ where k is an integer)

$$\frac{V_{out}}{V_{pp}} \approx [\delta_2 + 2\delta_2\rho(t-\tau_D)] - [\delta_2 + 2\delta_2\rho(t)] - 2\sqrt{\left(\frac{1}{4}-\delta_1^2\right)\left(\frac{1}{4}-\delta_2^2\right)}\Delta\phi(t,\tau_D) \quad (16)$$

where $\delta_{\{1,2\}} = 0.5 - \alpha_{\{1,2\}} << 0.5$ and can be neglected. Hence

$$\frac{V_{out}}{V_{pp}} \approx \frac{\Delta\phi(t,\tau_D)}{2}. \quad (17)$$

The corresponding PSD S_{out} is the Fourier transform of the autocorrelation of $V_{out}(t)$, which can be written as [21]

$$S_{out}(f) = \frac{V_{pp}^2}{4Z_L}\tau_D^2\frac{\sin^2\pi f\tau_D}{(\pi f\tau_D)^2}4\pi^2 S_{\Delta\nu}(f) \quad (18)$$

where $Z_L = 50$ Ohm is the input impedance of the spectrum analyzer and $S_{\Delta\nu} = FT\{<\phi'(t+\tau)\phi'(t)>_t\}$ is the phase noise spectrum. For the spectral range where the fundamental linewidth dominates, we have $S_{\Delta\nu}(f) = (\Delta\nu_{ST}/\pi)$.

IV. Experiment Results and Data Analysis

To measure the linewidth variation with respect to laser power, we first set up the experiment as discussed in the previous section. The toroid Raman laser was made by first fabricating a silica microdisk from a 2-μm thermal silica thin film on a silicon wafer using conventional photolithography/etching technology. The microdisk is then reshaped by a CO_2 laser into a toroid shape with surface roughness reduced to atomic scale. The fabricated toroid typically has an outer diameter of 50–100 μm depending on the etching conditions. It typically displays a Q above 100 million. In our application, however, we selected toroids of Q in the range of 50 million to suppress the split mode formed by Rayleigh scattering. To find the resonance wavelength of the pump, we coarse-tune the wavelength of the tunable laser while linearly scanning the wavelength in the range of 0.1 nm as shown in Fig. 1(a) using a waveform generator. The Raman laser signal is then detected by a balanced detector. The corresponding waveform on the oscilloscope is shown in inset II of Fig. 1(b). As shown, the signal detected by the balanced detector varies bidirectionally as a function of the optical frequency. Further, in inset I of Fig. 1(b) we illustrate the signals of the forward output pump power after a 20-dB optical attenuator (purple line) and Raman power tapered out by a 10% coupler (yellow line). We further record the pump (pink line) and laser (green line) power in the backward direction using a circulator. As indicated in the plot, the forward and backward Raman lasers have equal power. In addition, a pump threshold of 450 μW is observed while a minimum threshold of 68 μW is obtained on a different toroid laser. To study the frequency noise spectrum, we turn off the waveform generator and tune the pump laser in resonance to the toroid manually. When Raman lasing occurs, the balanced signal shown in inset III of Fig. 1(b) fluctuates around zero

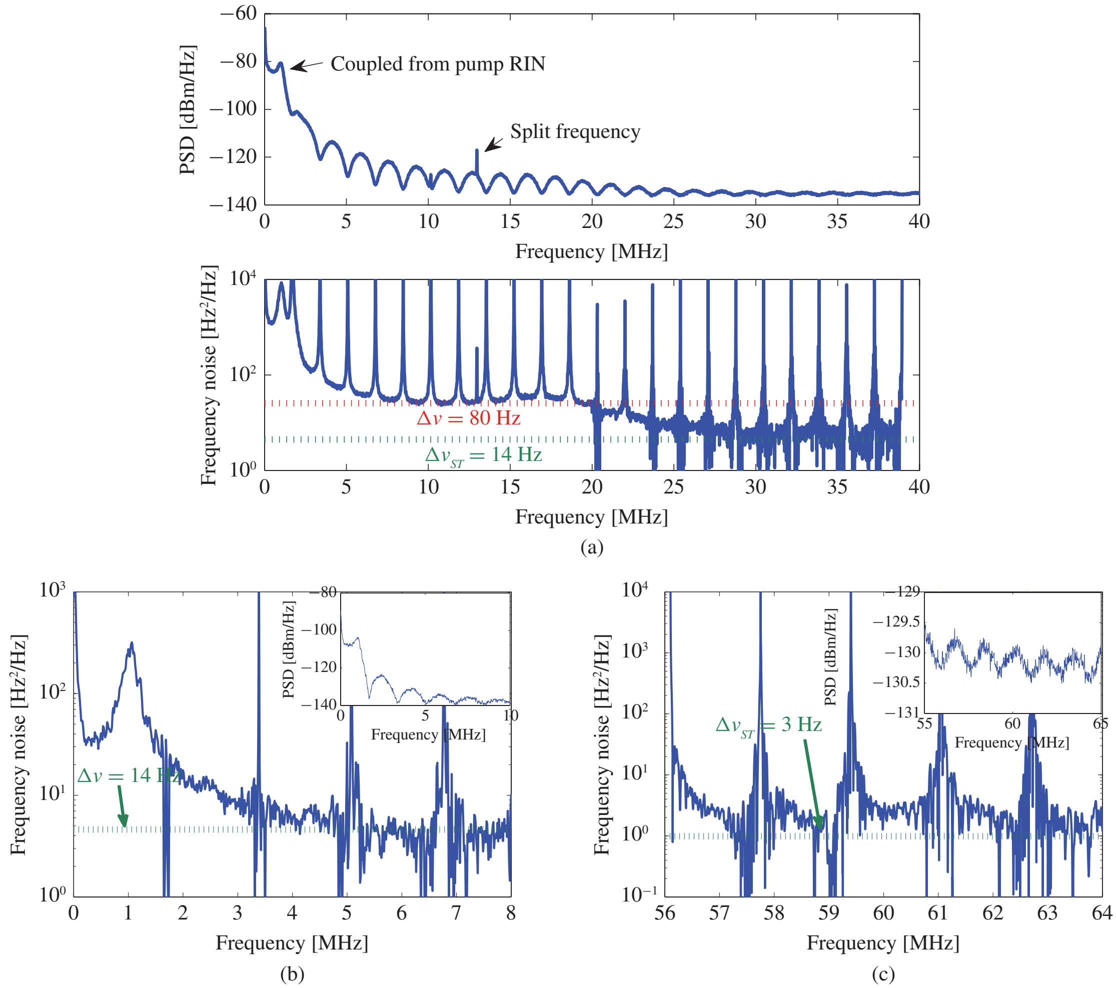

Fig. 2. (a) Power spectrum (upper plot) and extracted frequency noise spectrum derived from (18) (lower plot) in the frequency range 0–40 MHz. (b) Technical frequency noise observed below 8 MHz. (c) Quantum frequency noise measured at 56–64 MHz. The inset plots in (b) and (c) are the corresponding spectra measured from the analyzer.

due to the frequency drift. To measure the frequency noise at the quadrature point, we trigger the spectrum analyzer to start measurement when the balanced signal detected on the oscilloscope hits zero. Alternatively, if the output waveform varies rapidly during the acquisition period due to large frequency drifts and small free-spectral range, we carry out the acquisition in the regular spectral analysis mode under free-run condition. Consequently, a factor of 2 correction should be added to the spectrum due to averaging [22]. The upper plot of Fig. 2(a) displays the PSD of the frequency noise of a toroid Raman laser. To obtain a lower technical noise, here we used an NP Photonics fiber laser operating at 1538 nm and measured the Raman lasing at 1630 nm. We set the resolution bandwidth to 20 kHz and divide the frequency span into 0–40 MHz. The optical delay $\tau_D = 0.59$ μs is estimated by taking the inverse of the free-spectral range $f_{FSR} = 1.694$ MHz observed on the PSD curve. We further extracted the frequency noise $S_{\Delta\nu}(f)$ according to (18). As shown in the lower plot of Fig. 2(a), technical noises of 80 Hz dominate at frequencies below cavity bandwidth while quantum limit frequency noise dominates at frequencies above the cavity bandwidth. Fig. 2(b) and (c) display the lowest technical noises of 14 Hz and fundamental linewidth of 3 Hz measured on two other different toroids. The fundamental linewidth of 3 Hz is the lowest obtainable among on-chip lasers according to our knowledge. To verify the coupling of pump and laser intensity noise to the Raman frequency noise spectrum, we measured the RINs of the pump (red line) and the laser (blue line), which are shown in Fig. 3(a). We then constructed the expected frequency noises (blue line) according to (12) and compared them with the measured frequency noise (red line) in Fig. 3(b). Here, to facilitate the verification, we chose a toroid that exhibited strong relaxation oscillation peaks and pumped it by a new focus-tunable laser which introduced a larger intensity noise. The comparison shows excellent agreement.

Fig. 4(a) displays the fundamental linewidth versus inverse laser output power for three different toroids. The linear relationship derived from the plot shows good agreement with the Schawlow–Townes formula in (13). In Fig. 4(b), we further investigate the weak peak in the laser intensity noise spectrum shown in Fig. 3(a). We identify the peak as originating from the relaxation oscillation, as a linear relation between the oscillation frequency and square root of the laser power is observed. However, we find that the relaxation oscillation frequency is shifted 13.8 MHz higher than predicted in the

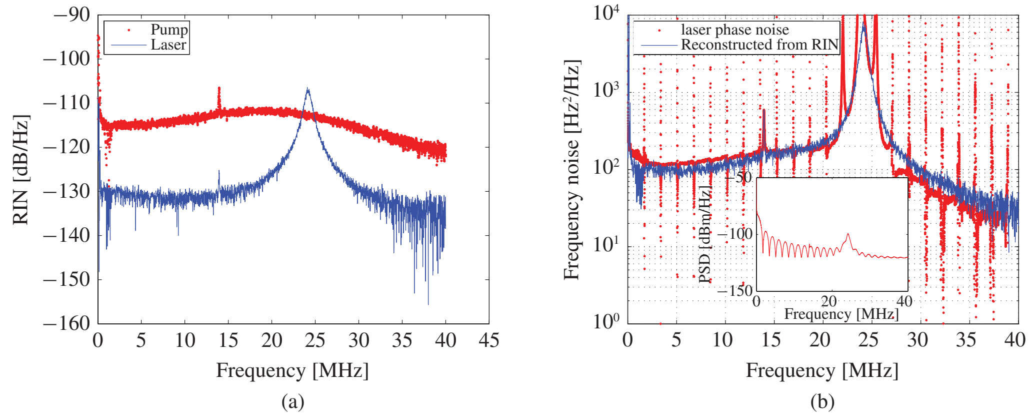

Fig. 3. (a) RINs of the pump and Raman laser and (b) comparison of the measured laser frequency noise and the noise spectrum constructed from pump and Raman RIN.

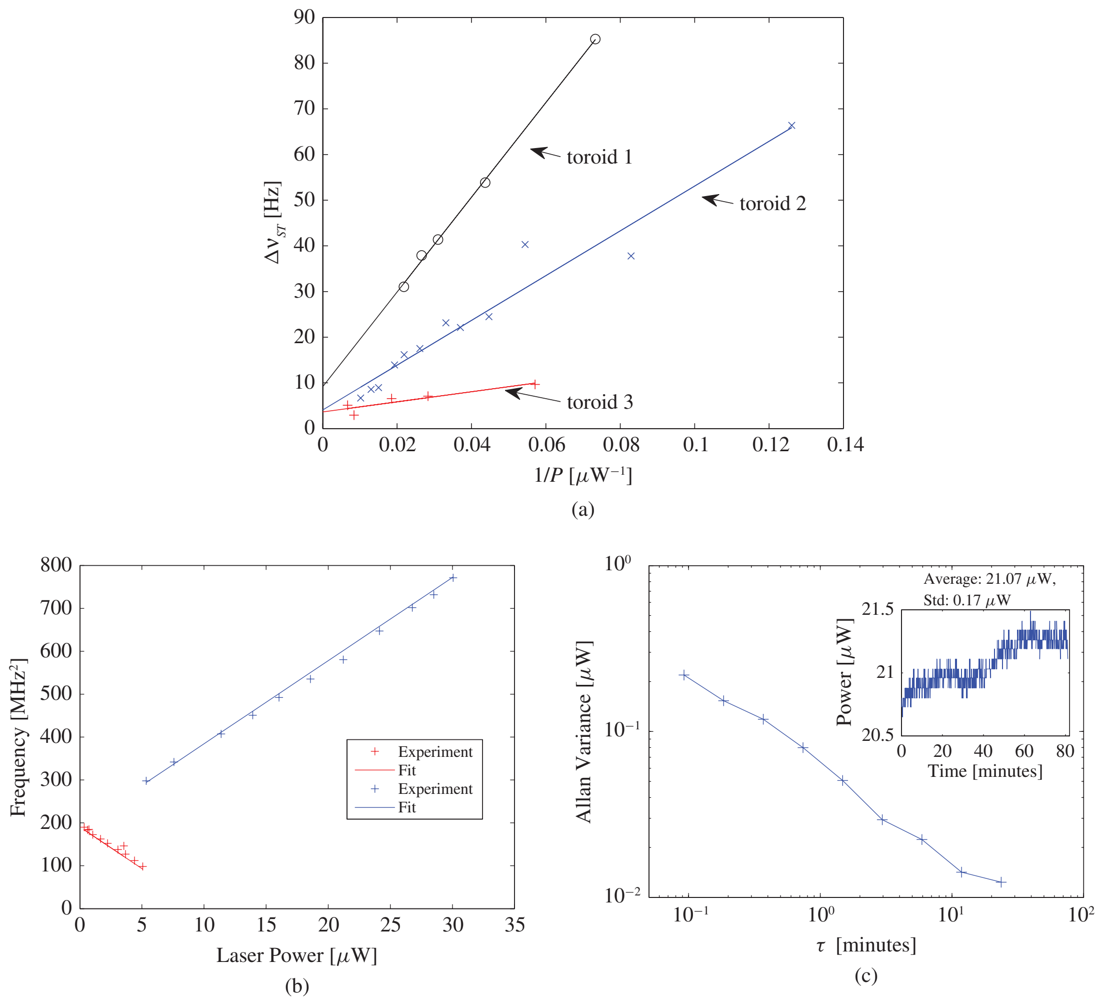

Fig. 4. (a) Fundamental linewidth versus inverse power. (b) Square of relaxation oscillation frequency as a function of laser optical power. (c) Allan variance of laser power (inset is the optical power as a function of time).

semiclassical model and split into two branches. We also find a small peak at the center frequency, which corresponds to the splitting mode existing in the ultrahigh-Q cavity. This verifies the relaxation oscillation conversion from he split frequency $|\beta_s|$ as predicted in (11). To test the stability of our Raman laser under the free-run condition, we allowed the toroid to lase in the CW mode for 90 min. As plotted in the inset of Fig. 4(c), an average power of 21 μW is obtained with a standard deviation of 0.17 μW. The Allan variance plot is further shown in the main plot.

V. Conclusion

In conclusion, we have demonstrated an on-chip Raman laser with fundamental linewidth as narrow as 3 Hz. We have found that a coherent discriminator method is suitable to measure ultranarrow-linewidth laser sources where the frequency drift is usually orders of magnitude larger than the laser linewidth itself. Our theoretical analysis also predicts that linewidth of sub-hertz level is possible due both to the ultrahigh Q and to high power of the Raman laser. An order of magnitude enhancement of the measured fundamental linewidth versus the theoretical prediction has also been observed, indicating the existence of excess spontaneous noise.

REFERENCES

[1] C. Spiegelberg, J. Geng, Y. Hu, Y. Kaneda, S. Jiang, and N. Peyghambarian, "Low-noise narrow-linewidth fiber laser at 1550 nm," *J. Lightw. Technol.*, vol. 22, no. 1, pp. 57–62, Jan. 2004.

[2] J. Geng, S. Staines, Z. Wang, J. Zong, M. Blake, and S. Jiang, "Highly stable low-noise Brillouin fiber laser with ultranarrow spectral linewidth," *IEEE Photon. Technol. Lett.*, vol. 18, no. 17, pp. 1813–1815, Sep. 1, 2006.

[3] H. Rong, R. Jones, A. Liu, O. Cohen, D. Hak, A. Fang, and M. Paniccia, "A continuous-wave Raman silicon laser," *Nature*, vol. 433, no. 7027, pp. 725–728, Feb. 2005.

[4] V. Sandoghdar, F. Treussart, J. Hare, V. Lefèvre-Seguin, J.-M. Raimond, and S. Haroche, "Very low threshold whispering-gallery-mode microsphere laser," *Phys. Rev. A*, vol. 54, no. 3, pp. R1777–R1780, Sep. 1996.

[5] D. K. Armani, T. J. Kippenberg, S. M. Spillane, and K. J. Vahala, "Ultrahigh-Q toroid microcavity on a chip," *Nature*, vol. 421, pp. 925–928, Feb. 2003.

[6] L. Yang, T. Lu, T. Carmon, B. Min, and K. J. Vahala, "A 4-HZ fundamental linewidth on-chip microlaser," in *Proc. Conf. Lasers Electro-Opt.*, Baltimore, MD, May 2007, pp. 1–2.

[7] M. L. Gorodetsky, A. D. Pryamikov, and V. S. Ilchenko, "Rayleigh scattering in high-Q microspheres," *J. Opt. Soc. Amer. B*, vol. 17, no. 6, pp. 1051–1057, Jun. 2000.

[8] T. Carmon, H. G. L. Schwefel, L. Yang, M. Oxborrow, A. D. Stone, and K. J. Vahala, "Static envelope patterns in composite resonances generated by level crossing in optical toroidal microcavities," *Phys. Rev. Lett.*, vol. 100, no. 10, pp. 103905-1–103905-4, Mar. 2008.

[9] B. Min, T. J. Kippenberg, and K. J. Vahala, "Compact, fiber-compatible, cascaded Raman laser," *Opt. Lett.*, vol. 28, no. 17, pp. 1507–1509, Sep. 2003.

[10] T. J. Kippenberg, S. M. Spillane, B. Min, and K. J. Vahala, "Theoretical and experimental study of stimulated and cascaded Raman scattering in ultrahigh-Q optical microcavities," *IEEE J. Sel. Topics Quantum Electron.*, vol. 10, no. 5, pp. 1219–1228, Sep./Oct. 2004.

[11] T. J. Kippenberg, S. M. Spillane, D. K. Armani, and K. J. Vahala, "Ultralow-threshold microcavity Raman laser on a microelectronic chip," *Opt. Lett.*, vol. 29, no. 11, pp. 1224–1226, Jun. 2004.

[12] C. Patel, "Linewidth of tunable stimulated Raman scattering," *Phys. Rev. Lett.*, vol. 28, no. 11, pp. 649–652, Mar. 1972.

[13] K. Vahala and A. Yariv, "Semiclassical theory of noise in semiconductor lasers–Part I," *IEEE J. Quantum Electron.*, vol. 19, no. 6, pp. 1096–1101, Jun. 1983.

[14] K. Vahala and A. Yariv, "Semiclassical theory of noise in semiconductor lasers–Part II," *IEEE J. Quantum Electron.*, vol. 19, no. 6, pp. 1102–1109, Jun. 1983.

[15] K. J. Vahala, "Dynamic and spectral features of semiconductor lasers," Ph.D. dissertation, Dept. Appl. Phys., California Inst. Technol., Pasadena, May 1985.

[16] A. Schawlow and C. H. Townes, "Infrared and optical masers," *Phys. Rev.*, vol. 112, no. 6, pp. 1940–1949, Dec. 1958.

[17] C. H. Henry, "Theory of the linewidth of semiconductor lasers," *IEEE J. Quantum Electron.*, vol. 18, no. 2, pp. 259–264, Feb. 1982.

[18] P. Goldberg, P. W. Milonni, and B. Sundaram, "Theory of the fundamental laser linewidth," *Phys. Rev. A*, vol. 44, no. 3, pp. 1969–1985, Aug. 1991.

[19] D. Dahan and G. Eisenstein, "The properties of amplified spontaneous emission noise in saturated fiber Raman amplifiers operating with CW signals," *Opt. Commun.*, vol. 236, nos. 4–6, pp. 279–288, Mar. 2004.

[20] P. Roos, S. Murphy, L. S. Meng, J. L. Carlsten, T. Ralph, A. G. White, and J. Brasseur, "Quantum theory of the far-off-resonance continuous-wave Raman laser: Heisenberg–Langevin approach," *Phys. Rev. A*, vol. 68, no. 1, pp. 013802-1–013802-12, Jul. 2003.

[21] D. Derickson, *Fiber Optic Test and Measurement* (Hewlett-Packard Professional Books). Upper Saddle River, NJ: Prentice Hall, 1998.

[22] L. Wei, "Study of optical phase lock loops and the applications in coherent beam combining and coherence cloning," Ph.D. dissertation, Dept. Appl. Phys., California Inst. Technol., Pasadena, 2008.

Tao Lu received the B.Sc. degree from the Department of Physics, University of Manitoba, Winnipeg, MB, Canada, in 1995, the M.Sc. degree from the Department of Electrical and Computer Engineering, Queen's University at Kingston, Kingston, ON, Canada, in 1998, and the Ph.D. degree from the Department of Physics, University of Waterloo, Waterloo, ON, in 2005.

He has worked in various companies including Nortel Networks, Kymata Canada, Peleton, and others, all in Ottawa, ON, Canada, on optical communications. He was a Post-Doctoral Fellow at the Department of Applied Physics, California Institute of Technology, Pasadena, from 2006 to 2008. He is currently an Assistant Professor at the Department of Electrical and Computer Engineering, University of Victoria, Victoria, BC, Canada. His current research interests include optical microcavities and their applications to ultranarrow-linewidth laser sources and single-molecule/nano-particle detection.

Lan Yang received the M.S. degree in materials science and the Ph.D. degree in applied physics from the California Institute of Technology, Pasadena, in 2000 and 2005, respectively.

She is currently an Assistant Professor in the Preston M. Green Department of Electrical and Systems Engineering, Washington University, St. Louis, MO. Her current research interests include novel photonic materials and ultrahigh-quality optical resonators for lasing, sensing, and nonlinear optics.

Dr. Yang was the recipient of the National Science Foundation CAREER Award in 2010 for her work on real-time particle detection.

Tal Carmon received the Ph.D. degree in physics from the Technion-Israel Institute of Technology, Haifa, Israel.

He was a Postgraduate Researcher at the California Institute of Technology, Pasadena, and is now an Assistant Professor at the University of Michigan, Ann Arbor. His current research interests include light-structure interaction via radiation pressure to control microdevices and light-matter interaction to produce high harmonics of light.

Bumki Min received the B.S. and M.S. degrees in electrical engineering from Seoul National University, Seoul, Korea, in 1999 and 2001, and the M.S. and Ph.D. degrees in applied physics from the California Institute of Technology (Caltech), Pasadena, in 2003 and 2006, respectively.

He is currently an Assistant Professor in the Department of Mechanical Engineering, Korea Advanced Institute of Science and Technology, Daejeon, Korea. After graduation, he worked as a Post-Doctoral Scholar at Caltech and also at the University of California, Berkeley. His current research interests include metamaterials, plasmonics, and optomechanics.